EurJIC
European Journal of Inorganic Chemistry

Research Article
doi.org/10.1002/ejic.202300634

Chemistry Europe
European Chemical Societies Publishing

www.eurjic.org

High Inhibition for a Co^{II} Tetrazole Bi-pyrazole Dinuclear Complex against *Fusarium Oxysporum* f. sp. *Albedinis*

Yousra Bahjou,[a, b] Smaail Radi,*[a] Mohamed El Massaoudi,[a] Youssef Draoui,[a] Nayarassery N. Adarsh,[c] Haralampos N. Miras,[d] Marilena Ferbinteanu,[e] Koen Robeyns,[b] Sabir Ouahhoud,[f, g] Redouan Benabbes,[f] Kai C. Hultzsch,[h] Mariusz Wolff,[h] and Yann Garcia*[b]

New coordination compounds made of two novel tetrazole and C,N-bipyrazole ligands, 2-(3,5,5′-trimethyl-1′H-[1,3′-bipyrazol]-1′-yl)acetonitrile (**L1**), and 1′-((1H-tetrazol-5-yl)methyl)-3,5,5′-trimethyl-1′H-1,3′-bipyrazole (**HL2**), were prepared and fully characterized by spectroscopic techniques. Their crystal structures were identified by single-crystal X-ray diffraction revealing mononuclear complexes: $[Ni(\mathbf{L1})_3](ClO_4)_2$ (**1**), $[Cd(\mathbf{L1})_2Cl_2]$ (**2**), $[Cu(\mathbf{HL2})(\mathbf{L2})]ClO_4$ (**3**), $[Cu(\mathbf{L2})_2]$ (**4**) and a dinuclear complex $[Co_2(\mathbf{HL2})(\mathbf{L2})Cl_3]$ (**5**) comprising Co^{II} ions in octahedral and tetrahedral surrounding within the same unit. Noticeably, **3** and **4** show different architectural structures due to ligand deprotonation as well as the effect of the counter anion. All compounds demonstrated antimicrobial activity against Gram (+) bacteria *Listeria innocua* and *Staphylococcus aureus*, as well as Gram (−) bacteria such as *Escherichia coli* and *Pseudomonas aeruginosa*, and antifungal activity against pathogenic fungi *Geotrichum candidum*, *Aspergillus niger*, and *Penicillium crustosum*. Interestingly, a high inhibition activity of 97% was reached for **5** with a low concentration of only 81.1 µmol/L against *Fusarium oxysporum* f. sp. *Albedinis*, which is commonly damaging palm trees crops.

Introduction

Pyrazole-based precursors have raised great interest due to their use in a variety of fields with broad socio economic implications, such as pharmaceutics and biology, catalysis, corrosion inhibition,[1–3] and environmental studies.[4–7] The incorporation of a tetrazole ring to produce a pyrazole-tetrazole platform can lead to a variety of applications, based on medicinal chemistry,[8,9] catalysis,[10] energetic materials,[11,12] magnetism,[13] spin crossover,[14] chemical sensing,[15,16] luminescent properties,[17] to name but a few. On the other hand, metal complexes are gaining popularity as a promising alternative to traditional organic antibiotics.[18] Their efficiency has been well documented in oncology,[19,20] and neurodegenerative

[a] Y. Bahjou, Prof. Dr. S. Radi, Prof. Dr. M. El Massaoudi, Y. Draoui
LCAE, Department of Chemistry
Faculty of Science, University Mohamed I
P.O. Box 524, Oujda 60 000 (Morocco)
E-mail: s.radi@ump.ac.ma

[b] Y. Bahjou, Dr. K. Robeyns, Prof. Dr. Y. Garcia
Institute of Condensed Matter and Nanosciences
Molecular Chemistry
Materials and Catalysis (IMCN/MOST)
Université catholique de Louvain
Place Louis Pasteur 1
Ottignies-Louvain-la-Neuve, 1348 Louvain-la-Neuve (Belgium)
E-mail: yann.garcia@uclouvain.be

[c] Dr. N. N. Adarsh
Chemistry and Biomolecular Science
Clarkson University
8 Clarkson Ave.
Potsdam, NY 13699 (USA)

[d] Prof. Dr. H. N. Miras
School of Chemistry, Joseph Black Building
University of Glasgow
Glasgow G12 8QQ (UK)

[e] Prof. Dr. M. Ferbinteanu
Marilena Ferbinteanu
Inorganic Chemistry Department
Faculty of Chemistry, University of Bucharest
Panduri Road, no. 90
Bucharest 050663 (Romania)

[f] Dr. S. Ouahhoud, Prof. Dr. R. Benabbes
Laboratory of Biochemistry and Biotechnology
Department of Biology, Faculty of Science
University Mohamed I
P.O. Box 524
Oujda 60 000 (Morocco)

[g] Dr. S. Ouahhoud
Present address: Laboratory of Biological Engineering
Team of Functional and Pathological Biology
Faculty of Sciences and Technology
Faculty of Medicine and Pharmacy
University Sultan Moulay Slimane
Beni Mellal 23000 (Morocco)

[h] Prof. Dr. K. C. Hultzsch, Dr. M. Wolff
Institut für Funktionelle Materialien und Katalyse
Fakultät für Chemie, Universität Wien
Währinger Straße 38–42
1090 Wien (Austria)

Supporting information for this article is available on the WWW under https://doi.org/10.1002/ejic.202300634

Research Article
doi.org/10.1002/ejic.202300634

diseases,[21] due to their greater variety of geometries and a higher tridimensionality than most organic compounds.[22] Up to now, a wide range of Cu^{II}, Co^{II} and Cd^{II} complexes with azole based donor ligands have shown remarkable antifungal and antibacterial activities,[23–25] together with a low toxicity.[9]

A vascular disease caused by the fungal infection of *Fusarium oxysporum* f. sp. is causing several damages to cash crops including banana, garlic, tomato and palm all over the world.[26] For example, *Fusarium oxysporum* f. sp. *albedinis* (Foa) named as 'Bayoud disease' is a great cause of loss of dates in North Africa,[27,28] thus threatening local economy as well as exportations. A recent prediction anticipate that the bacteria could spread out through Middle Eastern and European countries for the years 2050 and 2100.[26] As a solution, several specific compounds have been proposed to stimulate the plant defense system against pathogen attack, such as some heterocyclic ligands,[29,30] and coordination complexes.[9,31,32] It is still however challenging to develop efficient compounds capable of high inhibitory activity at low concentration.

In an effort to investigate the coordinative ability and the effect on the structural morphology of produced molecular species, a new family of coordination compounds with selected first row transition metals was prepared by designing two new ligands, **L1** and **HL2** (Scheme 1), that incorporate both pyrazole and tetrazole rings (Scheme 2 and 3). Single crystal X-ray diffraction allowed to isolate the following complexes: [Ni-(**L1**)$_3$](ClO$_4$)$_2$ (**1**), [Cd(**L1**)$_2$Cl$_2$] (**2**), [Cu(**HL2**)(**L2**)]ClO$_4$ (**3**), [Cu(**L2**)$_2$] (**4**) and [Co$_2$(**HL2**)(**L2**)Cl$_3$] (**5**). Hirshfeld surface analyses were performed for **1**–**5** to evaluate in much detail the distribution of hydrogen bonds and intermolecular interactions in the crystal structures. Furthermore, these compounds were tested against gram (–) bacterial strains (*Escherichia coli*, *Pseudomonas aeruginosa*), gram (+) strains (*Staphylococcus aureus*, *Listeria innocua*), and their antifungal pathogen activities (*Geotrichum candidum*, *Aspergillus niger*, *Penicillium crustosum* and *Fusarium oxysporum*

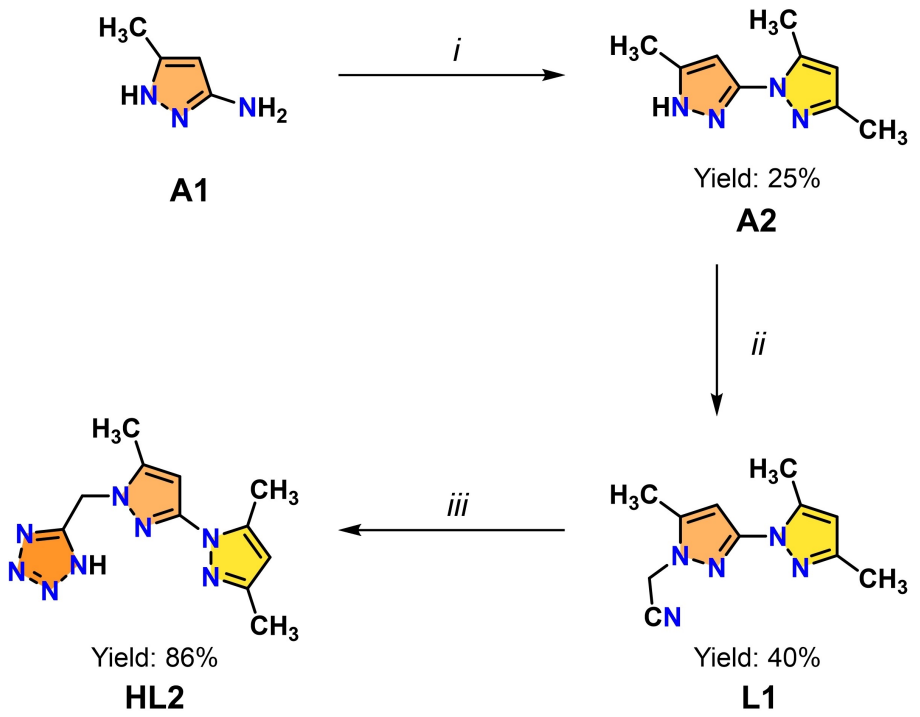

Scheme 1. Synthesis of bipyrazole (**L1**) and tetrazole (**HL2**) ligands. (*i*) NaNO$_2$/HCl, ascorbic acid, acetylacetone. (*ii*) *t*-BuOK, 2-chloroacetonitrile, diethyl ether, reflux. (*iii*) NaN$_3$, ZnCl$_2$, H$_2$O, reflux (110 °C, 4–5 h).

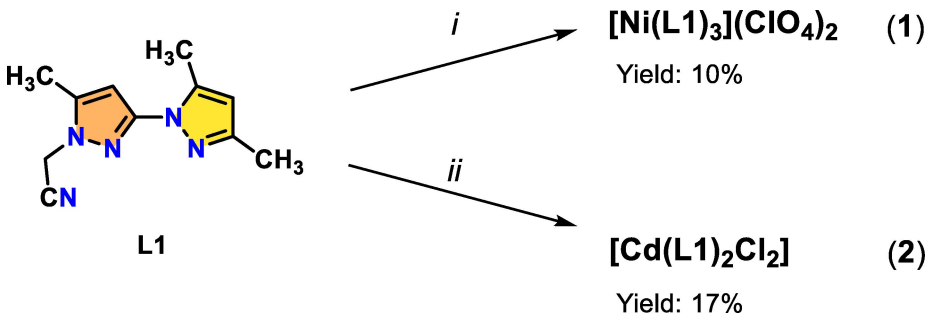

Scheme 2. Synthetic pathways for the preparation of coordination complexes **1** and **2** from **L1**. (*i*) Ni(ClO$_4$)$_2$·6H$_2$O. (*ii*) CdCl$_2$·H$_2$O.

Research Article
doi.org/10.1002/ejic.202300634

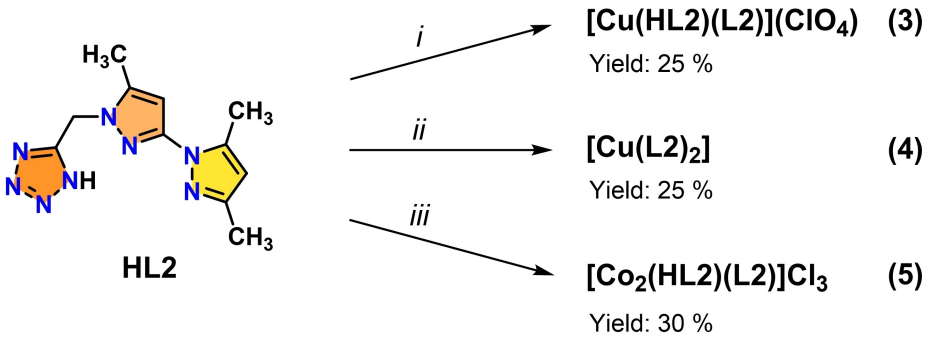

Scheme 3. Synthetic pathways leading to complexes **3–5** from **HL2.** ***i***) $Cu(ClO_4)_2 \cdot 6H_2O$. ***ii***) $CuCl_2$. ***iii)*** $CoCl_2 \cdot 2H_2O$.

f.sp. albedinis). Remarkable activities were observed against *Fusarium oxysporum* f.sp. *albedinis* extracted from sick palm trees presenting the 'Bayoud disease'.[33]

Result and Discussion

The combinatorial effect of pyrazole-tetrazole is attractive given the potential ability to afford several coordination modes and to generate intricate coordination networks with diverse architectures. We herein aimed to prepare bi-pyrazole-tetrazole ligands due to their involvement in numerous weak interactions such as steric hindrance, π-stacking etc. which could give rise to a variety of crystal lattices. The synthetic protocol involved three steps (Scheme 1): i) a condensation of 5-methyl-1H-pyrazol-3-amine with pentane-2,4-dione, in the presence of sodium nitrite and ascorbic acid in distilled HCl/H_2O, to lead to 3,5′5′-trimethyl′1′H-1′3′-bipyrazole (**A2**).[34] (ii) alkylation of **A2** with 2-chloroacetonitrile in the presence of potassium tert-butylate (*t*-BuOK) as a base with diethyl ether solvent to yield to 2-(3,5′5′-trimethyl′1′H-[1′3′-bipyrazol]′1′-yl)acetonitrile (**L1**). (iii) cyclization of **L1** with sodium azide in the presence of $ZnCl_2$ in distilled water to lead to 1′-((1H-tetrazol-5-yl)methyl)-3,5′5′-trimethyl′1′H-1′3′-bipyrazole (**HL2**) as a white powder.

The reaction of **L1** with $Ni(ClO_4)_2 \cdot 6H_2O$ in hot acetonitrile, with a ligand/metal ratio of 3:1, followed by diethyl ether diffusion, afforded single crystals of the mononuclear nickel(II) complex (**1**) with three ligands coordinated in a bidentate fashion. **2** was obtained by reacting **L1** with $CdCl_2 \cdot H_2O$ in hot methanol in a 2:1 molar ratio to yield a powder which was recrystallized with a few drops of water/acetonitrile to afford X-ray quality single crystals (Scheme 2).

The reaction of **HL2** with the copper salts $Cu(ClO_4)_2 \cdot 6H_2O$ and $CuCl_2$, respectively, was carried out separately in a 2:1 ratio in a solution of $HClO_4$ (5%) and HCl (5%), respectively. The reaction resulted in the formation of single crystals by slow evaporation of **3** and **4**. On the other hand, the synthesis of **5** was carried out by treatment of **HL2** with $CoCl_2$ using a molar ratio (1:1) in HCl (5%) solution. Pink single crystals of **5** were successfully obtained by slow evaporation (Scheme 3).

The chemical and phase purity of complexes **1–5** was verified by elemental analysis and powder X-ray diffraction by comparing the experimental PXRD patterns with the simulated ones from single-crystal X-ray (SXRD) data (Figure S17). Such batches of single crystals were then used to register the FT-IR as well as diffuse reflectance spectra. FT-IR spectra of **L1**, **HL2** and their complexes, show characteristic bands centred at 3153, 2990, 2352 and 1550 cm^{-1} (Figs S18, S19), which are attributed to N–H vibrations of pyrazole, aromatic C–H, nitrile C≡N and aromatic C=C groups, respectively. The same bands were found shifted in **1** and **2**. Four characteristic bands were identified for **HL2**: the first one at 3137 cm^{-1}, for the N–H of the tetrazole group, and the band at 2920 cm^{-1}, characteristic of the elongation vibration of the aromatic C–H in the pyrazole ring. The third characteristic band at 1642 cm^{-1} was assigned to the C=N vibrations of pyrazole and tetrazole groups. The fourth band at 1553 cm^{-1} originates from the C=C stretching vibration of the pyrazole unit. Comparison of the IR spectra of the ligand with its complexes shows that the N–H band of the tetrazole group is shifted by 21 cm^{-1} (**3**), 12 cm^{-1} (**4**) and 3 cm^{-1} (**5**), respectively. This clearly shows the involvement of the tetrazole unit in the coordination. In contrast, non-coordinated perchlorate anions were found at 1095 cm^{-1} and 1086 cm^{-1} for **1** and **3**, respectively.

Diffuse reflectance UV-vis spectra of **L1** and **HL2** display a major band at $\lambda = 228$ nm and a weak band at $\lambda = 265$ nm, successively, ascribed to π→π* and n-π* transitions (Figures S20–S21). After complexation, the maximum absorption bands concerning the intra-ligand π→π* transitions, show a slight shift due to the increased conjugation of the system, which also leads to the increase in intensity of the largest peaks. In addition, complexes **1–5** show typical metal-ligand charge transfer (MLCT) absorption bands between $\lambda = 279$ and 323 nm (Figures S20–21), which are attributed to charge transfer to metals (dπ(M)) and **L1** and **HL2** ligands (π*). On the other side, weak bands centred at 427, 600, 495 nm, respectively in **4**, **1** and **5** are relevant to d–d transitions.

Structural analysis by single crystal X-ray diffraction of **1** revealed a mononuclear complex of formula $[Ni(\mathbf{L1})_3](ClO_4)_2$, which crystallizes in the triclinic system (space group *P*-1). The asymmetric unit consists of one nickel atom with three coordinated **L1** ligands and two non-coordinating perchlorate counter-ions. The nickel centre is in a distorted octahedral environment [∠N–Ni–N = 76.97(6)–97.87(7)°] composed of six nitrogen atoms of three bidentate ligands. The ligands are arranged in a way that the complex shows a 3-fold (C_3)

Research Article
doi.org/10.1002/ejic.202300634

symmetry axis. The asymmetry of the ligand is also reflected in the Ni–N bond lengths. Bond lengths between Ni^{II} and N atoms of the pyrazole rings substituted by methyl $–CH_3$ groups at positions 3 and 5 are 2.0732(17), 2.0744(16) and 2.0997(17) Å, while those between Ni^{II} and N atoms of the pyrazole rings substituted by cyanoethyl $–C_2H_4CN$ group at position 1 are longer and 2.1170(17), 2.1314(16) and 2.1572(17) Å (Table S5, Figure 1a).

$CdCl_2$ reacted with **L1** to form a mononuclear complex $[Cd(\mathbf{L1})_2Cl_2]$ (Figure 1b), which crystallizes in the monoclinic system (space group *C*2/*c*). The $[Cd(\mathbf{L1})_2Cl_2]$ (Figure 2a) complex is found on a crystallographic 2-fold axis, thus the asymmetric unit comprises half of the formula moiety. The octahedral structure is a *cis* complex with respect to the chloride atoms and the acetonitrile substituted pyrazole rings are in *trans* position. The bond angle values involving both nitrogen atoms of a bidentate ligand (65.62(6)°) are largely responsible for the distortion of the octahedral environment of the central cadmium atom (Table S6). The crystal packing of **2** is mainly determined by π···π stacking and C–H···Cl between pyrazole rings of the ligand and $–CH_2$ group of the ligand and chloride bounded to the metal centre, respectively (Figure 2a and 2b).

The octahedral distortion parameters (**ζ, Σ, Θ**) were calculated to quantify the degree of distortion from a perfect octahedral geometry around the M^{II} centre in **1** and **2**. Distortion parameters ζ, Σ and Θ are 0.158 Å, 87.66° and 272.07° for **1**; and 0.484 Å, 114.17° and 398.78° for **2**;[35] all these values lie in the expected range observed for distorted quasi-octahedral M^{II} complexes.[36–40]

Compound **3** crystallizes in the triclinic space group *P*-1. The asymmetric unit of **3** consists of one copper atom, two ligands (one **HL2** ligand is coordinated in a bidentate fashion *via* two pyrazole nitrogen atoms and the other one **L2** (deprotonated form) is coordinated in a tridendate fashion with additional coordination through the tetrazole nitrogen atom to the Cu^{II} centre) and one perchlorate counter-anion with $Z=2$. The copper atom is located at the centre of a square pyramidal geometry, surrounded by four pyrazole and one deprotonated tetrazole nitrogen atoms of the two **HL2/L2** ligands (Figure 3A). The bond lengths between the copper centre and the pyrazole nitrogen atoms fall in the range of 1.948(2)−2.359(2) Å, while the $Cu–N_{tetr}$ is at 1.964(2) Å (Table S7).

The use of chloride instead of perchlorate afforded complex **4** also crystallizing in the *P*-1 space group (Figure 3b). Unlike **3**, both ligands are deprotonated, still forming a similar complex

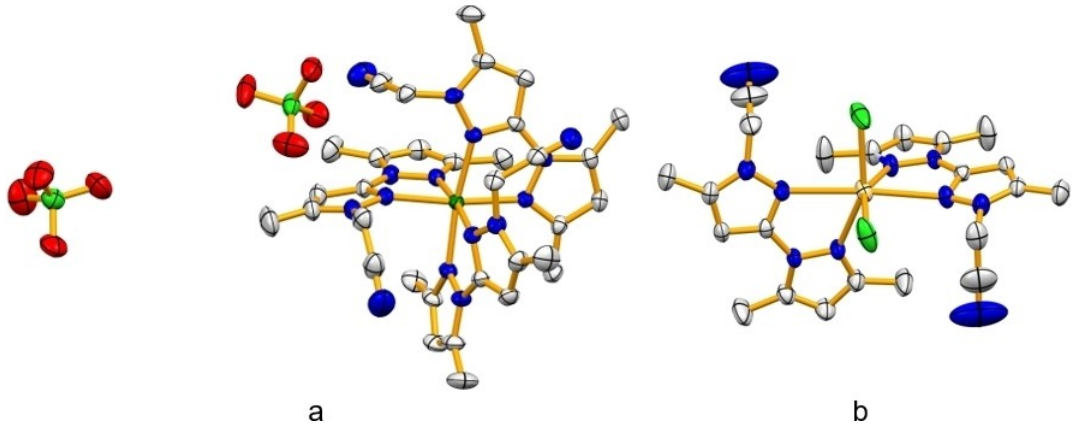

Figure 1. ORTEP representation of **1** (a) and **2** (b) with thermal ellipsoids drawn at the 50% probability level, the complex is oriented along the pseudo C_3 axis. Colour code: Ni, dark green; Cd, light yellow; C, light grey; N, dark blue; O, red; Cl, light green.

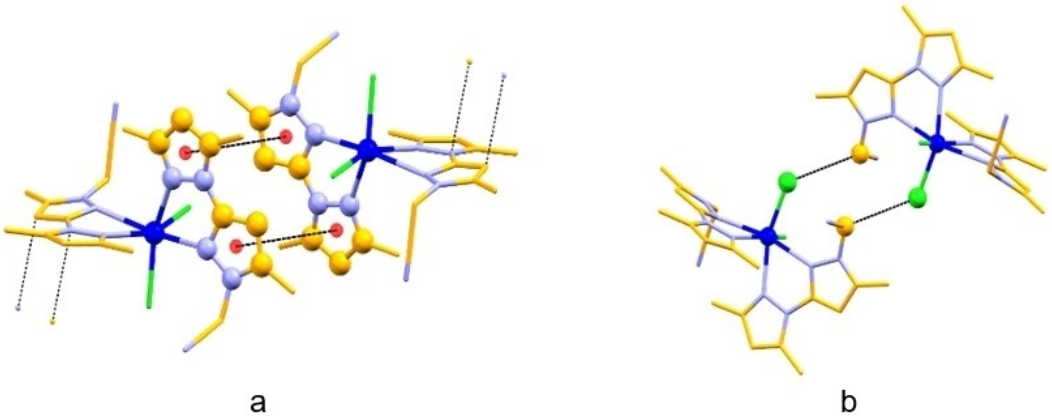

Figure 2. Crystal structure illustration of **2**: a) π···π stacking between two adjacent molecules of **2** in the unit cell; b) C–H···Cl hydrogen-bonding interaction; Colour code: Cd, dark blue; C, yellow; N, blue; Cl, green.

Research Article
doi.org/10.1002/ejic.202300634

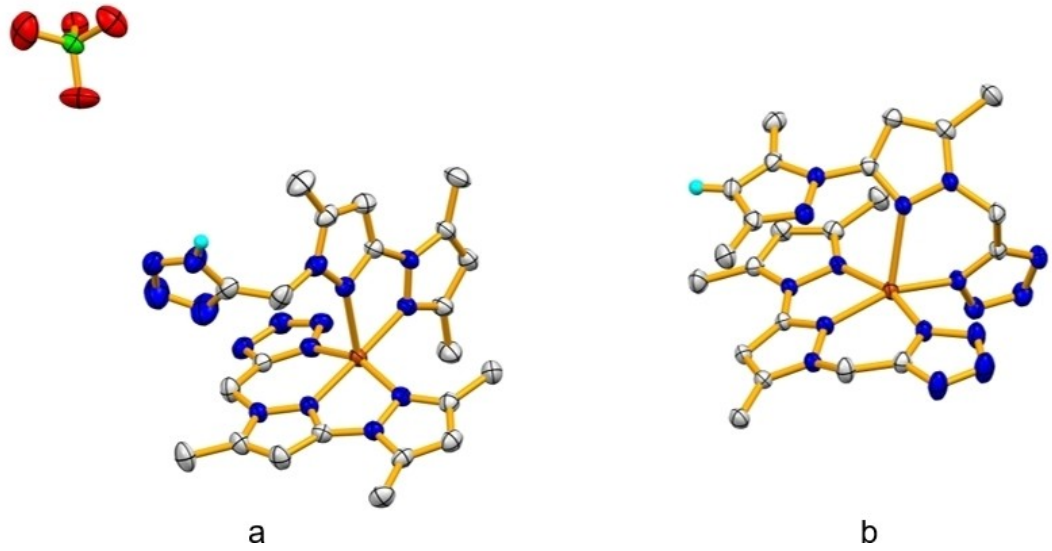

Figure 3. ORTEP representation of: **3** (a) and **4** (b) with displacement ellipsoids drawn at the 50% probability level; Colour code: Cu, brick red; C, light grey; N, dark blue; O, red; Cl, light green.

with the central Cu atom in a near perfect square pyramidal geometry. The observed Cu–N_{pyr} bond lengths are in the range between 1.982(2) and 2.338(1) Å, and for Cu–N_{tetr} at 1.982(1)–1.999(2) Å (Table S8).

In Cu^{II} complexes **3** and **4**, the copper ion has a five-coordinated environment. Addison *et al.* defined and quantified a geometric parameter τ_5 to five–Coordinate metal system as an index of the degree of distortion.[41] The τ_5 value is defined by the equation $|\beta\text{-}\alpha|/60$, where β and α variables are the two greatest coordinate angles of the polyhedron. The $\tau_5 = 0.34$ for **3** and 0.08 for **4**, which indicates a small deviation from the ideal square-pyramidal geometry with C_{4v} symmetry ($\tau_5 = 0$).[41]

Complex **5** crystallizes in a monoclinic system, space group $P2_1/c$. Contrary to **3** and **4**, both ligands act as tridentate coordinating ligands. One of the ligands, **L2** (in a deprotonated form), acts as a bridging unit between the Co(**HL2**) unit and the cobalt atom coordinated to three chlorides, resulting in the formation of a dinuclear complex (Figure 4a). The distance between these two cobalt centres is 6.068 Å. Two different coordination environments (distorted octahedra and tetrahedra) are found within the same complex. Bond valence analysis and the overall charge balance indicate both cobalt atoms in the Co^{II} state. Co_1 shows a distorted octahedral geometry with distortion parameters ζ, Σ and Θ of 0.214 Å, 133.10° and 538.95°, respectively. The distances between the Co(1) metal centre and the nitrogen atoms of pyrazole and tetrazole are 2.088(4)–2.194(4) Å and 2.138(4)–2.112(4) Å, respectively, while the average Co(2)–Cl bond lengths range from 2.239(2) Å to 2.258(2) Å and Co(2)–N_{tetr} is 2.070(4) Å (Table S9). The second cobalt ion is in a near perfect tetragonal environment.[43] Houser's four-coordinate τ_4 index is the sum of angles α and β – the two largest θ angles in the four-coordinate species – subtracted from 360°, all divided by 141°. The τ_4 parameter is calculated to be 0.96 for **5** indicating an almost ideal tetrahedral

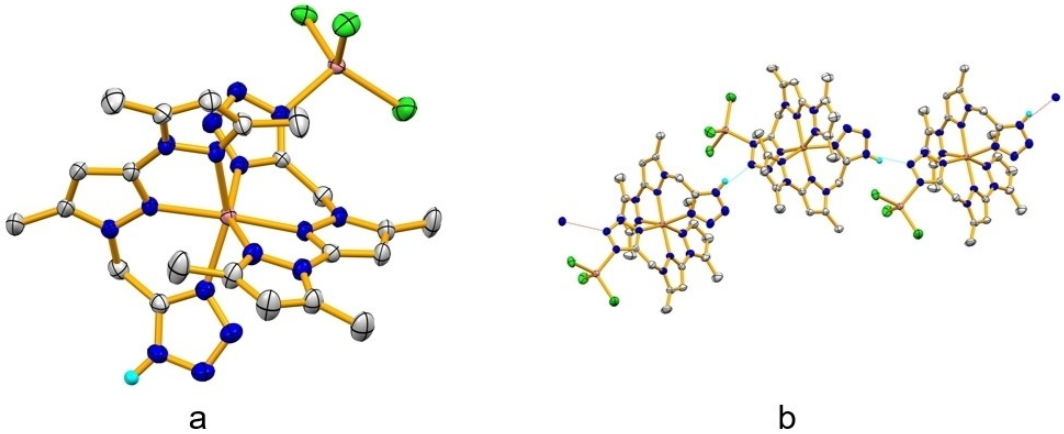

Figure 4. a) ORTEP representation of **5**, with displacement ellipsoids drawn at the 50% probability level; **b**) hydrogen bonded 1D chain. Colour code: Co, pink; C, light grey; N, dark blue; Cl, light green.

Research Article
doi.org/10.1002/ejic.202300634

geometry ($\tau_4 = 0$) with D_{4v} symmetry.[42] The dinuclear Co^{II} complexes recognize each other through N–H···N hydrogen bonding [N8–H···N15 = 2.926(8) Å, ∠N8–H–N15 = 159.68°] involving the tetrazole functionalities of the metal bound ligands leading to a 1D hydrogen bonded *zig-zag* chain (Figure 4b).

The Hirshfeld surface (HS) analysis determines the surface or space occupied by a molecule or ion in the crystal structure in which the electron density of the crystal is divided by molecular fragments of electron densities; i.e., the surface where the electron density $\rho_{il}(r)$ of the molecule is larger than the electron density $I_{xt}(r)$ of the adjacent molecule. From the HS plots (Figure 5) and two-dimensional (2-D) fingerprint (FP) plots,[43,44] one can quantify the nature of the intermolecular interactions present in the crystal structure. More detailed HS plots are given in Figure S22.

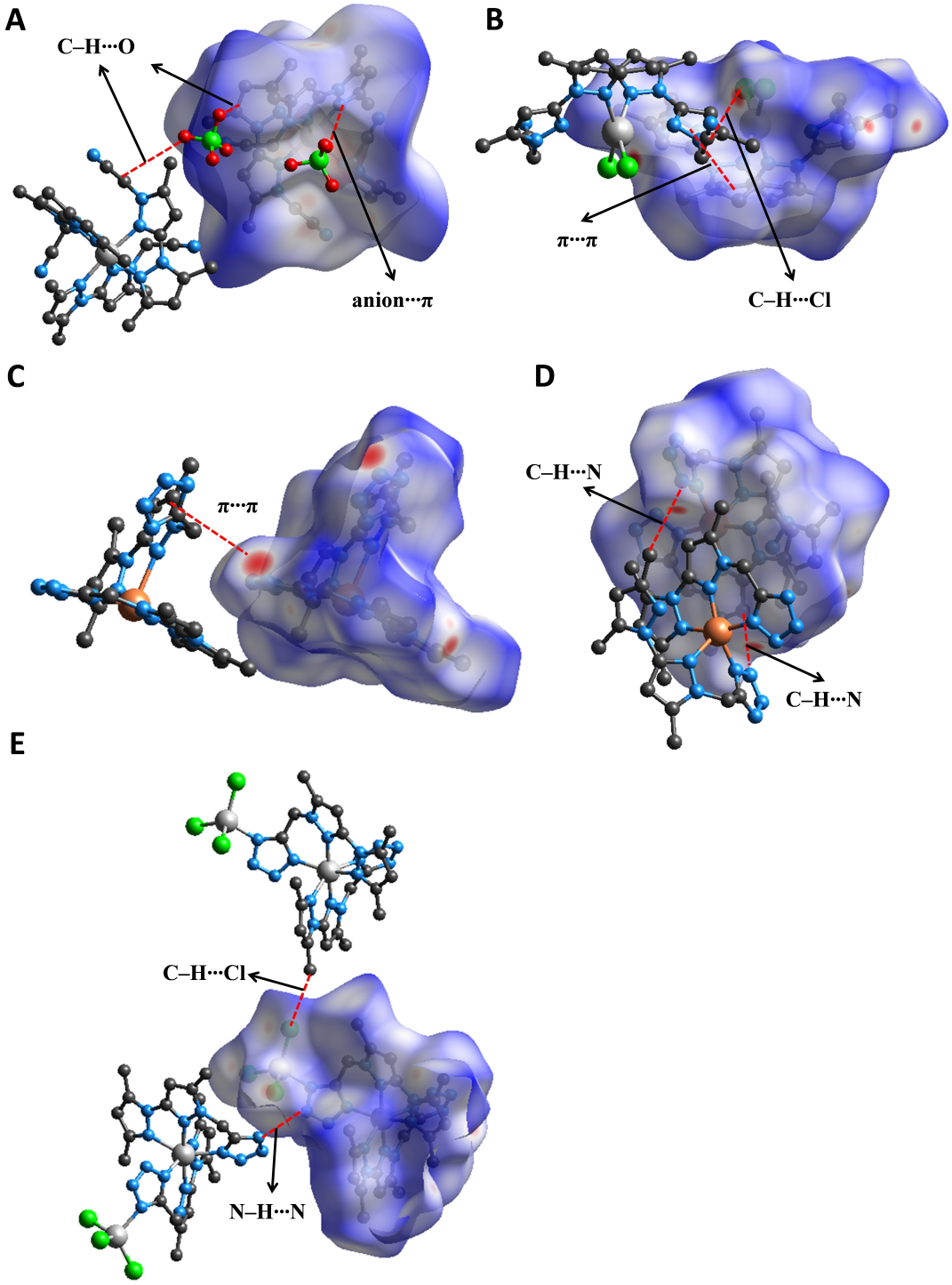

Figure 5. Hirshfeld Surfaces of compounds **1** (A), **2** (B), **3** (C), **4** (D), **5** (E). Red, white and blue spots belong to intermolecular contacts less than, equal to and larger than the van der Waal radii, respectively; supramolecular interactions (red dotted lines) for each compound is also shown.

Research Article
doi.org/10.1002/ejic.202300634

HS of **1** showed a surface having of area 689.99 Å^3, which is spread over 976.10 Å^3 in which the surface was generated between −1.1844 a.u. (red spot) and 3.1551 a.u. (blue colour); the shape index plot and curvedness plot are generated from –0.9983 to 0.9991 a.u. and −4.1655 to 0.6829 a.u., respectively. The presence of short contacts of **1** with its adjacent molecule through C–H···O hydrogen bonding (O···H/H···O = 23.8 %) and anion···π interactions (O···C/C···O = 1.1 %, C···H/H···C = 6.7 %) containing $-CH_2-$ and nitrile groups/pyrazole rings, of ligand with perchlorate anion are detected in the 2-D FP of **1** (Figure S23). Moreover, the molecule **1** is also involved in various van der Waals contacts [N···H/H···N = 14.7 %, H···H = 44.5 %, N···C/C···N = 1.1 %] with neighbouring molecules.

The HS of **2** deposited an area of 508.19 Å^3 and accumulated a volume of 656.55 Å^3 having the scaled colour gradient on the HS generated in between −0.1546 a.u. (red colour) and 1.4057 a.u. (blue colour); the shape index plot and curvedness plot are created from −0.9979 a.u. to 0.9974 a.u. and −3.5373 a.u. to 0.3127 a.u., respectively. The 2-D FP revealed that the intermolecular interactions were present in between inside and outside HS of **2** in which the molecule interacts with each other via π···π stacking involving pyrazole rings of the ligand [C···C = 1.2 %, C···H/H···C = 14.1 %] and C–H···Cl hydrogen-bonding interactions involving the $-CH_2-$ of ligand with metal bound chloride ion [Cl···H/H···Cl = 17.8 %]. The complex **2** is also stabilized by various weak supramolecular interactions [H···H = 40.0 %, N···C/C···N = 2.9 %, N···H/H···N = 23.6 %] (Figure S24).

The HS analysis revealed that **3** is covering an area of 480.83 Å^3 and a volume of 611.00 Å^3 in which the scaled colour gradient on the HS generated in between –0.2497 a.u. (red colour) and 1.1896 a.u. (blue colour); the shape index plot and curvedness plot are created from –0.9965 a.u. to 0.9992 a.u. and –3.9597 a.u. to 0.3694 a.u., respectively. The quantification of supramolecular contacts using D FP showed the presence of tetrazolate anion ring interactions [N···H/H···N = 28.5 %], C–H···O hydrogen-bonding [C···H/H···C = 11.0 %, O···H/H···O = 14.3 %] and anion···π interactions [C···C = 1.7 %, C···N/N···C = 2.4 %] participating by the ligand and perchlorate anions, and also other weak interactions [H···H = 36.1 %, O···N/N···O = 2.1 %] (Figure S25).

The HS of **4** showed an area and volume of 447.94 Å^3 and 607.50 Å^3, respectively. The scaled colour gradient on the HS generated in between −0.1710 a.u. (red colour) and 1.6845 a.u. (blue colour); the shape index plot and curvedness plot are created from −0.9928 a.u. to 0.9981 a.u. and −3.3566 a.u. to 0.3332 a.u., respectively. From the 2-D FP it is revealed that the quantity of N–H···O hydrogen bonding for the macrocycle formation and 1-D hydrogen bonding is 44.5 % in the crystal structure of **4**; other weak non-bonded interactions are also present [H···H = 42.2 %, C···N/N···C = 3.0 %, C···H/H···C = 7.8 %, C···C = 0.6 %] (Figure S26).

In the case of **5**, the HS spread over an area of 583.36 Å^3 and volume of 788.30 Å^3 in which the scaled colour code on the surface engendered in between −0.5202 a.u. (red colour) and 1.7424 (blue colour); the shape index plot and curvedness plot are created from −0.9973 a.u. to 0.9986 a.u. and −3.7305 a.u. to 0.7339 a.u., respectively. The presence of a 1-D hydrogen bonded corrugated sheet structure through N–H···N [N···H/H···N = 19.7 %] and C–H···Cl [Cl···H/H···Cl = 25.4 %] hydrogen bonding are confirmed and quantified using the 2-D FP; other weak interactions are also present in the crystal structure such as Cl···N/N···Cl = 4.0 %, H···H = 39.4 %, N···C/C···N = 1.0 % and C···C = 0.3 % (Figure S27). From the comparison plot of various common interactions in all the five complexes, it is revealed that more contributions of N···H/H···N, C···H/H···C and H···H are present in complex **4**, **2** and **1**, respectively (Figure 6).

Antibacterial activities

Screening of the antibacterial activities of **L1**-**HL2** and **1–5** against Gram (+) (*Listeria innocua* and *Staphylococcus aureus*) and Gram (−) (*Escherichia coli* and *Pseudomonas aeruginosa*) bacteria was evaluated. The average diameter of the inhibition zone (in mm) are shown in Table S1 and Figure 7. **HL2** showed the highest antibacterial activity against the tested bacteria with 10–15 mm areas. For example, **2**, **HL2** and **4** showed significant values of 11.5 mm, 13.65 mm and 12.9 mm, respectively for *Listeria innocua* (+). In contrast, **L1**, **1** and **3** presented intermediate-values (9–9.35 mm). In addition, **L1**-**HL2** and **1–4** showed noticeable activities against *Staphylococcus aureus* (+) with an inhibition zone similar to that obtained in *Listeria innocua* (+). For *Pseudomonas aeruginosa* (−), the studied compounds presented intermediate values (8.75–12 mm) in comparison to the reference drug (Gentamicin). Metal salts did not show any activities except the cadmium salt for two bacteria with moderate values (Figure 7). These results are however consistent with the pyrazole-tetrazole entities found in the literature.[45–47]

Antifungal activities

The antifungal activity of **L1, HL2** and their complexes **1–5** against the fungal strains *Geotrichum candidum*, *Aspergillus niger* and *Penicillium crustosum* was tested (Table S2 and Figure 8). **L1** has a noticeable antifungal activity against *Aspergillus niger* by 11 mm, whereas for **HL2**, a maximum value of 15.85 mm is reached. The Cd^{II} complex **2** shows high antifungal activity against the three strains compared to other metal complexes, which is also seen for $CdCl_2 \cdot H_2O$.[48] Complexes **3** and **5** also showed even higher activity against *Geotrichum candidum* compared to **HL2**, with values of 10.95 mm and 10.85 mm, respectively.

The activity of **2** is in the range of other reported Cd^{II} complexes (Table 1). It is however more active than the ligand **L1**. The complexation is expected to reduce the polarity of the metal ion due to the partial sharing of its positive charge with donor groups. Furthermore, the metal ion's lipophilic nature increases, thereby presumably promoting its permeability through the lipid layer of the cell membrane.[23,49,50] Dissociation of **2** in solution was excluded due to its inherent stability, e.g. as shown by high resolution mass spectrometry (Figure S12).

The anti-Fusarium activity of our synthesized compounds against *Fusarium Oxysporum* f. sp. *albidinis* was investigated too

Research Article
doi.org/10.1002/ejic.202300634

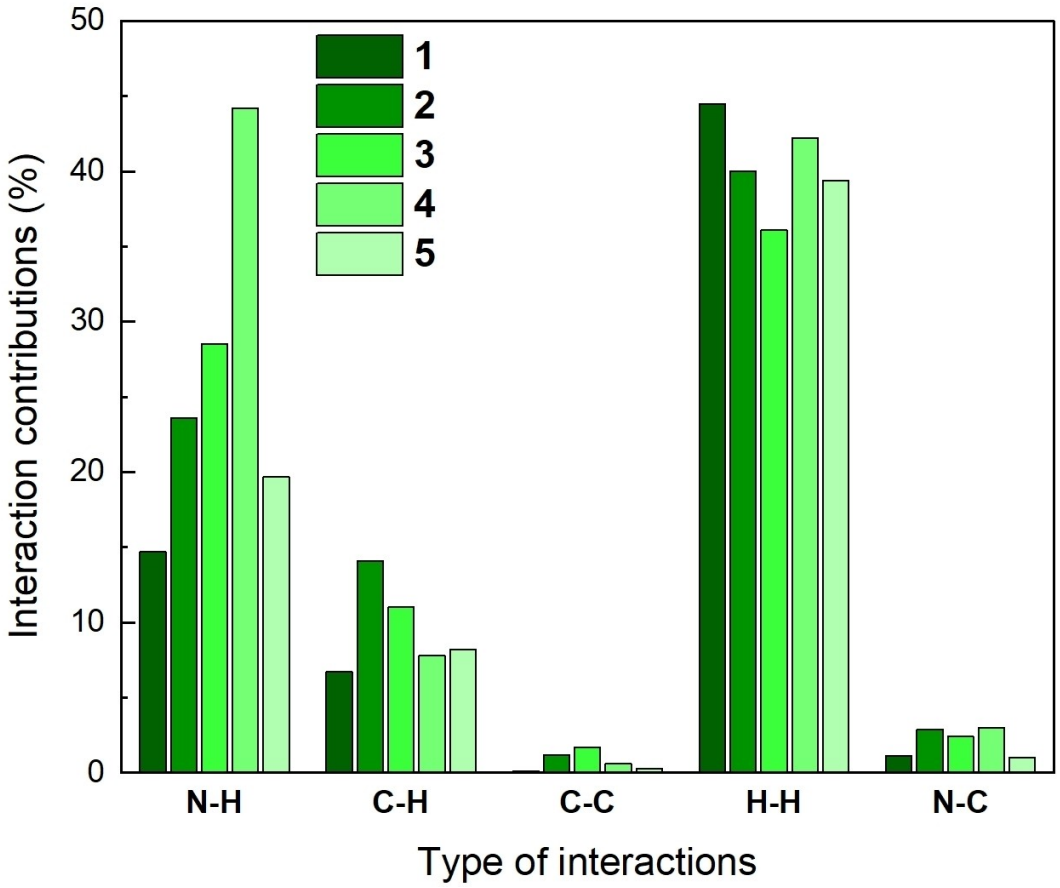

Figure 6. Contributions of various interactions in **1–5**.

(Table S3 and Figure 9). All of our compounds are remarkably active. **L1**, **HL2** and **5** display however exceptional values above 95% at a volume of only 150 μL (Table 2), compared to cycloheximide as positive control and to existing studies on pyrazole-tetrazole compounds.[57–59] Metal salts were also tested to check if the activity would be linked to the metal itself. This is moderately true for $CdCl_2 \cdot H_2O$ which shows superior activities compared to other salts, but stands much lower than the complex **5** or **HL2**.

Considering **5** and **HL2**, a distinction can be made given that the working concentration of complex **5** (81.1 μmol/L) is much lower than that of **HL2** (232.3 μmol/L), thus showing superior characteristics. Nevertheless, this high inhibition of 97% overcome previous findings (Table 2 and Table S3). This outcome could be attributed to enhanced electron delocalization across the dinuclear complex **5**, which would enhance the lipophilicity, ultimately disrupting the cellular respiration process. Consequently, this disruption may hinder protein synthesis, limiting the organism's growth, and ultimately leading to the demise of microorganisms.[60]

Conclusions

In summary, we have successfully synthesized and characterized five novel transition metal complexes, with new tetrazole bi pyrazole ligand. Complexes **3** and **4** exhibit distinct architectural differences due to ligand deprotonation and the influence of counter-anions. Complex **5** is a dinuclear complex holding both octahedral and tetrahedral sites within the same unit. These compounds demonstrate noticeable bacteriostatic activity against both Gram (+) and Gram (−) bacteria, as well as antifungal properties against a range of fungi. Particularly impressive is the remarkable 97% inhibition achieved by **5** at a concentration of only 81.1 μmol/L against *Fusarium oxysporum* f. sp. *albedinis*, the causing agent of Bayoud disease in palm trees. This success motivates further exploration of potential ligands of this substance class.

Experimental Section

Materials and instrumentation: Nuclear magnetic resonance (NMR) spectra were recorded at room temperature with a Bruker Avance II 300 MHz instrument. Chemical shifts (δ) are reported in parts per million (ppm) relative to residual DMSO-d_6 ($\delta = 2.50$ ppm for ^{1}H and 39.5 ppm for ^{13}C). Coupling constants are expressed in Hertz (Hz). The following abbreviations are used: s = singlet, d = doublet, dd =

Research Article
doi.org/10.1002/ejic.202300634

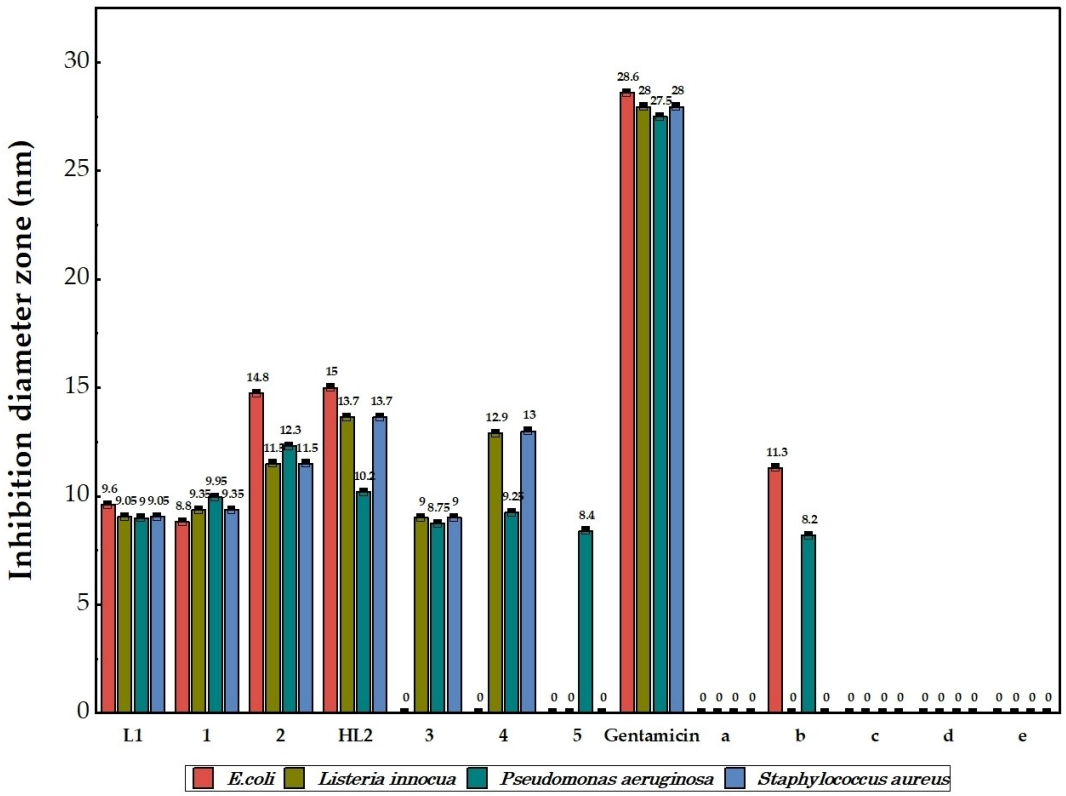

Figure 7. Antibacterial activity of **L1**, **HL2**, **1–5** and metal salts. ***a:*** $Ni(ClO_4)_2 \cdot 6H_2O$, ***b:*** $CdCl_2 \cdot H_2O$, ***c:*** $Cu(ClO_4)_2 \cdot 6H_2O$, **d**: $CuCl_2$ **e**: $CoCl_2 \cdot 2H_2O$. ***DMSO** has no effect.* Molar concentrations are given in Table S1.

doublet of doublets, t = triplet. High-resolution mass spectra (HRMS) of ligands **L1**, **HL2** and complexes **1** and **2** were recorded using a ThermoFisher Q-Exactive spectrometer using acetonitrile as solvent. High-resolution electrospray ionization mass spectra (HR-ESI-MS) of complexes **3–5** were recorded on a *maXis* QTOF-MS instrument (*Bruker Daltonics* GmbH, Bremen, Germany). Fourier transform-infrared (FT-IR) spectroscopy measurements were performed using an Equinox 55 (Bruker) equipped with a diamond ATR module and a mercury-cadmium-telluride (MCT) detector. The Bruker OPUS software was used for data processing (including ATR correction). The letters s, m and w denote the peak intensity as strong, medium and weak, respectively. UV-visible spectra were recorded using a Shimadzu 3600 plus spectrometer equipped with a Harrick's Praying Mantis™ modulus which allows direct analysis of powders in reflectance mode. Melting points were measured using a Kofler thermal bench. Powder X-ray diffraction (PXRD) patterns were collected on a D8-Advance diffractometer (Bruker, Germany) with Cu Kα radiation ($\lambda = 1.5148$ Å) operating at 40 kV and 30 mA. Elemental analyses (C, H, N, and O) were performed at the Microanalytical Laboratory of the University of Vienna for monoplicate or duplicate ~1 mg sample on an EA 3000 CHNS–O Elemental Analyser from Eurovector.

X-ray Crystallography: Single-crystal X-ray diffraction data of complexes **1** and **2** were recorded on an MAR345 image plate at room temperature, using MoK_α radiation ($\lambda = 0.71073$ Å) generated by an Incoatec microfocus source (Montel optics). Data integration and reduction was performed with the CrysAlis^{PRO} Software, Version 1.171.37.35 from Rigaku Oxford Diffraction and the implemented absorption correction was applied.[63] The structure was solved by SHELXT[64] and refined by least-squares against F^2 by SHELXT2018/3.[65] In **1**, the crystal structure contains a single solvent cavity accounting for 16.7% of the unit cell volume. The diffuse solvent region was identified by the SQUEEZE procedure in Platon.[66] Both ClO_4^- anions were found disordered over two sites. For one set of disordered anions the minor part has displacement ellipsoids constraint to be equal to the major part. One terminal C≡N group was found disordered as well and refined using geometry restraints. The minor part was refined with isotropic and rigid bond restraints.

Single-crystal X-ray diffraction data of complexes **3** and **4** were recorded on an Xcalibur/Oxford diffractometer equipped with a Sapphire 3 CCD detector and a 4-cycle Kappa geometry goniometer, using enhanced MoK_α ($\lambda = 0.71073$ Å) at 150 K equipped with a graphite monochromator. Analytical absorption correction was applied using CrysAlis RED software. CrysAlis CCD and CrysAlis RED software were used for data collection and data reduction/cell refinement, respectively. Structure solution and refinement were performed with SHELXS-2014,[67] and SHELXL-2014,[68] using the WinGX software package.[69] Corrections for the incident and diffracted beam absorption effects were applied using empirical absorption corrections.[70] Single-crystal X-ray diffraction data of complex **5** were collected on a Rigaku R-AXIS RAPID II diffractometer with MoK_α ($\lambda = 0.71075$ Å) radiation. The crystal structure was solved by direct methods[71] and refined by the full-matrix least-squares techniques [Least Squares function minimized: (SHELXL97) $w(F_o^2 - F_c^2)^2$ where w = Least Squares weights] on F^2 using the SHELXL package.[68] All calculations were performed using the Crystal Structure[72] crystallographic software package except for refinement, which was performed using SHELXL program.

All non-H atoms were refined anisotropically. Solvent molecules were found and included in the refinement of the structures. Final unit cell data and refinement statistics for **1–5** are collected in Table S4.

Research Article
doi.org/10.1002/ejic.202300634

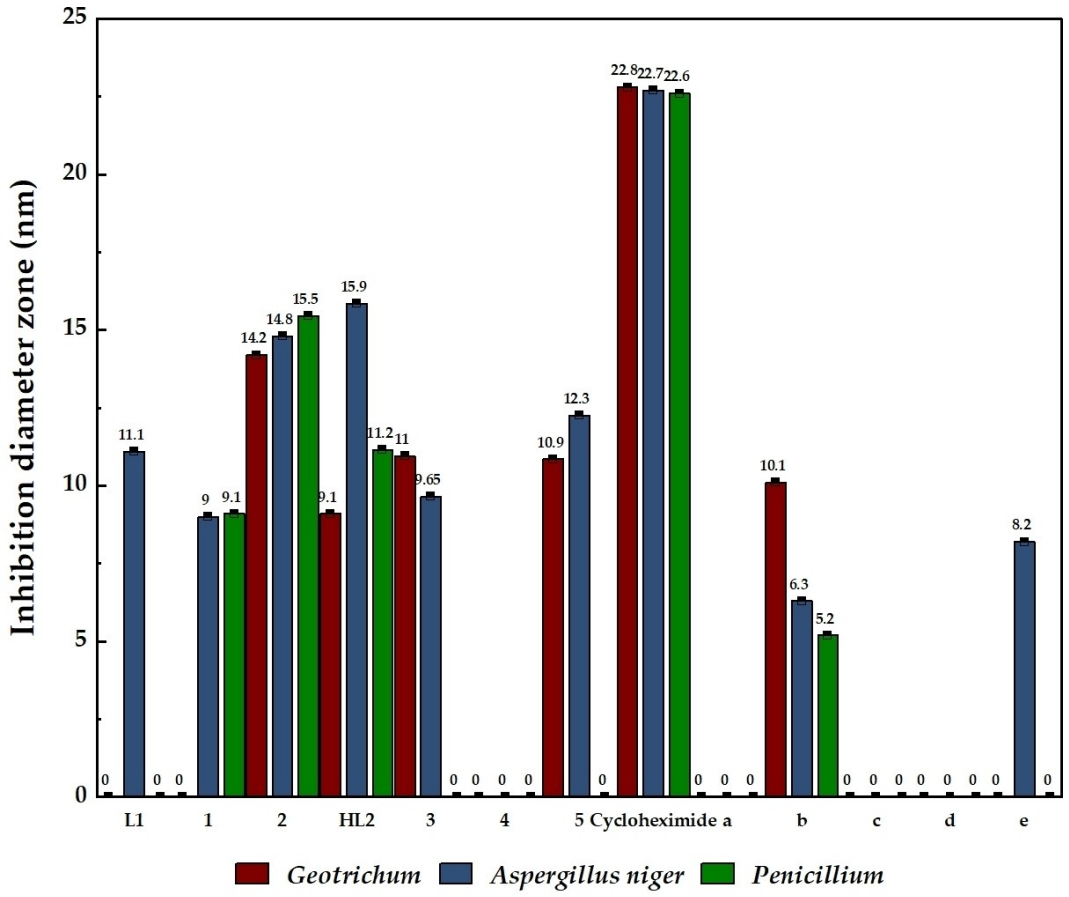

Figure 8. Antifungal activity of **L1, HL2**,**1**–**5** and metal salts. **a**: $Ni(ClO_4)_2 \cdot 6H_2O$, **b:** $CdCl_2 \cdot H_2O$, **c**: $Cu(ClO_4)_2 \cdot 6H_2O$, **d**: $CuCl_2$ **e**: $CoCl_2 \cdot 2H_2O$. ***DMSO** has no effect.* Molar concentrations are given in Table S2.

Deposition Number(s) 2263956–2263960 (for **1–5**) contain(s) the supplementary crystallographic data for this paper. These data are provided free of charge by the joint Cambridge Crystallographic Data Centre and Fachinformationszentrum Karlsruhe Access Structures service.

Synthesis section

Synthesis of 3,5,5′-trimethyl-1′H-1,3′-bipyrazole (A2): In a three-necked flask equipped with magnetic stirring and cooled to −2 °C, 3(5)-amino-5(3)-methyl pyrazole (**A1**) (5.39 g, 55.4 mmol, 1 eq.) and 12 M hydrochloric acid (24 mL) were introduced. A solution of sodium nitrite (4.62 g, 66.95 mmol, 1.2 eq.) in distilled water (6.92 mL) was added dropwise to the mixture. After 1 h of stirring at −2 °C, a solution of ascorbic acid (9.86 g, 55.98 mmol, 1 eq.) in distilled water (36 mL) was added slowly at −2 °C, followed by an addition of acetylacetone (5.6 g, 55.92 mmol, 1 eq.) and a few drops of ethanol. The ice bath was removed, and the reaction remained stirred for 48 h. The reaction mixture was neutralized with sodium carbonate solution. The organic phase was extracted three times with CH_2Cl_2, dried over sodium sulfate and evaporated to dryness. The residue obtained was purified on a silica column using (ethyl acetate/hexane: 8/2) as eluent. The desired product was precipitated in hexane (7 mL). Yield: 25 % (2.5 g). M. p. 114 °C. R_f 0.57 (Ethyl acetate/silica). ^{1}H NMR (300 MHz, DMSO–d_6, δ (ppm)): 12.45 (s, 1H, NH); 6.11 (dd, 1H, pz–H); 5.97 (s, 1H, pz–H); 2.36 (s, 3H, –CH_3); 2.25 (s, 3H, –CH_3); 2.14 (s, 3H, –CH_3).^{13}C NMR (50 MHz, DMSO–d_6): 150.06 (1 C, C–CH_3); 148.11(1 C, C–N); 139.96 (1 C, C–CH_3); 139.91 (1 C, C–CH_3); 13.88 (1 C, –CH_3); 11.20 (1 C, –CH_3); 13.08 (1 C, –CH_3).

Synthesis of 2-(3,5,5′-trimethyl-1′H-[1,3′-bipyrazol]-1′-yl) acetonitrile (L1): To a mixture of 3,5,5′-trimethyl-1′H-1,3′-bipyrazole (0.5 g, 2.85 mmol, 1 eq.) and *t*-BuOK (0.56 g, 3.38 mmol, 1.5 eq.) in diethyl ether (10 mL) heated to reflux for 1 h and then cooled to 0 °C, 2-chloroacetonitrile (0.18 mL, 1.33 mmol, 1.1 eq.) was slowly added. Then, the reaction mixture was refluxed again for 2 h, filtered and concentrated to dryness. The obtained residue was separated on silica column using a mixture (hexane/ethyl acetate :1/9) as eluent. The desired product was precipitated in a few milliliters of diethyl ether. Yield: 40 % (0.25 g). M.p. 150 °C. R_f 0.67 (ethyl acetate/silica). ^{1}H NMR (300 MHz, DMSO-d_6, δ (ppm)): 6.29 (d, J = 0.8 Hz, 1H, pz–H); 6.01 (s, 1H, pz-H); 5.42 (s, 2H, CH_2–CN); 2.39 (d, J = 0.7 Hz, 3H, –CH_3); 2.33 (d, J = 0.7 Hz, 3H, –CH_3); 2.14 (s, 3H, –CH_3). ^{13}C NMR (50 MHz, DMSO-d_6): 148.87 (1 C, C–CH_3); 149.67 (1 C, C–N); 141.82 (1 C, C–CH_3); 140.18 (1 C, C–CH_3); 116.29 (1 C, C≡N); 107.79 (1 C, C=C, pz); 99.91 (1 C, C=C, pz); 37.68 (1 C, –CH_2–CN); 13.87 (1 C, –CH_3); 13.05 (1 C, –CH_3); 11.11 (1 C, –CH_3). Selected IR frequencies (KBr disc, cm^{-1}): 3153 (w), 2990 (w), 2352 (w), 1550 (s). ESI-MS (+) *m/z*: 216.12452 $(M+H)^+$. Anal. Calcd. for **L1** ($C_{11}H_{13}N_5$): C, 61.38; H, 6.09; N, 32.54. Found: C, 61.05; H, 6.08; N, 32.31.

Synthesis of 1′-((1H-tetrazol-5-yl)methyl)-3,5,5′-trimethyl-1′H-1,3′-bipyrazole (HL2): A suspension of sodium azide (0.48 g, 4.4 mmol, 1 eq.), zinc chloride (1.02 g, 4.4 mmol, 1.5 eq.) and 2-(3,5,5′-trimethyl-1′H-[1,3′-bipyrazol]-1′-yl)acetonitrile (0.54 g, 3 mmol, 1 eq.) in water (60 mL) was heated to reflux for 12 h. After allowing the suspension to cool to room temperature, concentrated hydrochloric

Research Article
doi.org/10.1002/ejic.202300634

Table 1. Antimicrobial activity of complex **2** and other reference Cd^{II} complexes.

Metal Complexes	Bacteria and Fungi screened	Concentration (mol/L)	Activity Inhibition Zone (mm)	Ref.
2	*Escherichia coli (−)* *P. aeruginosa (−)* *S. aureus (+)* *Geotrichum* *Aspergillus niger*	$4.9\ 10^{-3}$	14 ± 0.75 12 ± 0.3 11 ± 0.5 14 ± 0.2 14 ± 0.8	This work
$[Cd(ahpnb)_2(H_2O)_2].4H_2O$[a] ahpnb 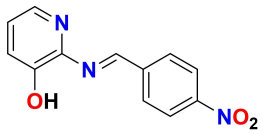	*Escherichia coli (−)* *Geotrichum*	$1.41\ 10^{-2}$	16 18	51
$[Cd(L)_2(NCS)_2]$[b] L 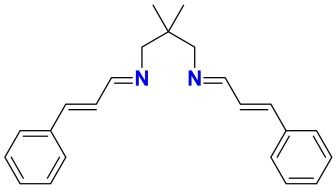	*Escherichia coli (−)* *P. aeruginosa (−)* *S. aureus (+)*	$2.24\ 10^{-2}$	11 ± 0.4 7 ± 0.5 11 ± 0.2	52
$[Cd(L)_2(N_3)_2]$[b] L 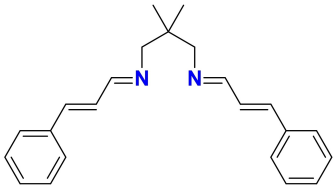	*Escherichia coli (−)* *P. aeruginosa (−)* *S. aureus (+)*	$2.33\ 10^{-2}$	11 ± 0.3 18 ± 0.3 6	52
$[CdCl_2(L)]$[c] L 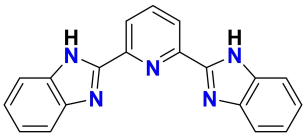	*Escherichia coli (−)* *P. aeruginosa (−)* *S. aureus (+)*	$6.08\ 10^{-2}$	18 13 24	53
$[Cd(L)_2]$[d] L 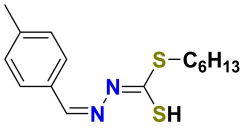	*Escherichia coli (−)*	$1.42\ 10^{-2}$	8	54
$[Cd(L)_2(caf)_2]$[e] L 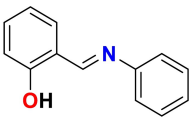 caf 	*Escherichia coli (−)* *S. aureus (+)* *Aspergillus niger*	$2.23\ 10^{-2}$	9 12 15	55

Research Article
doi.org/10.1002/ejic.202300634

Table 1. continued

Metal Complexes	Bacteria and Fungi screened	Concentration (mol/L)	Activity Inhibition Zone (mm)	Ref.
$[Cd(L)_2]^f$ L 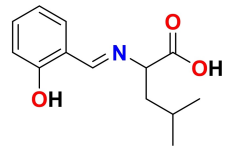	*Escherichia coli (−)* *S. aureus (+)* *Aspergillus niger*	-	6.75 ± 0.90 12.25 ± 1.5 6.20 ± 0.45	56

[a] ahpnb = ligand synthesized from ahp : 2-amino-3-hydroxypyridine and nb : 4-nitrobenzaldehyde. [b] L = 2,2-dimethyl-*N*,*N*′-bis-(3-phenyl-allylidene)-propane-1,3-diamine. [c] L = 2,6-bis(benzimidazol-2yl)pyridine. [d] L = Schiff base synthesized from S-hexyldithiocarbazate and 4-methylbenzaldehyde. [e] L = Salicylidene aniline; caf = caffeine. [f] L = Schiff base ligand ($C_{13}H_{17}NO_3$).

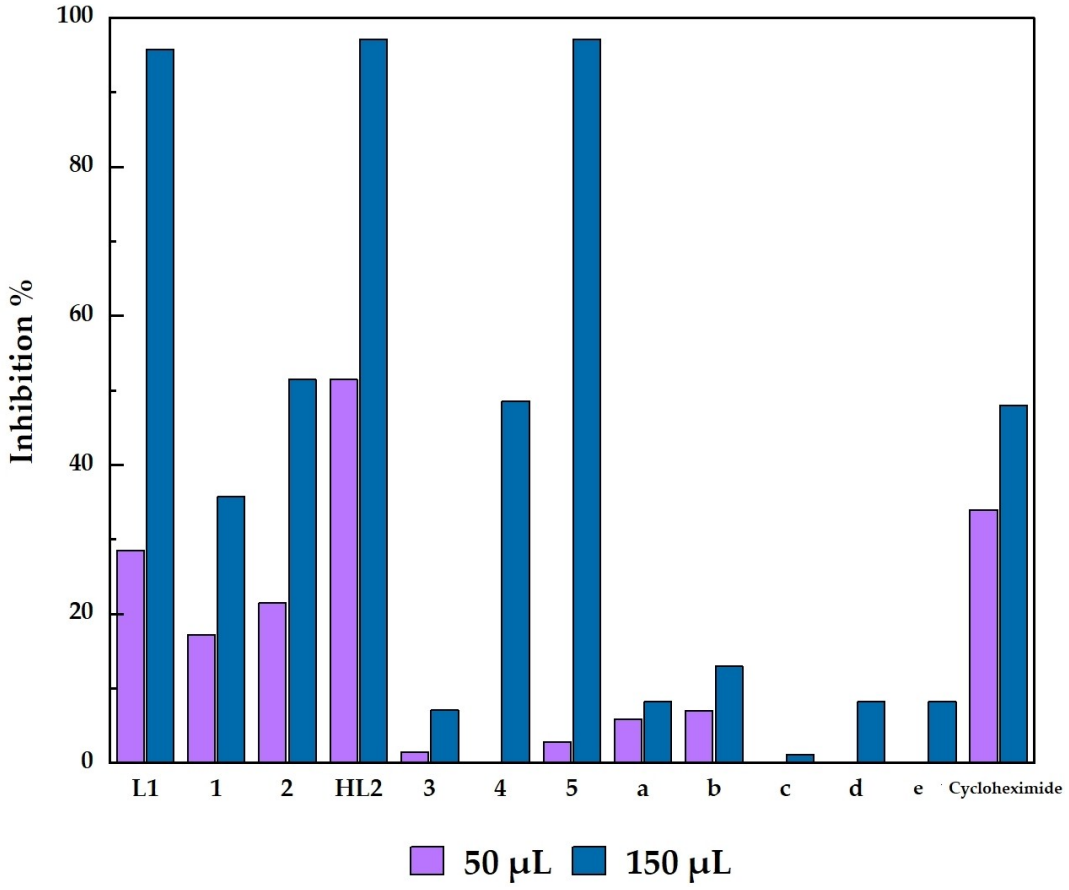

Figure 9. Inhibition of Fusarium growth activity of **L1, HL2**, **1–5**, positive control (cycloheximide) and metal salts. **a**: $Ni(ClO_4)_2 \cdot 6H_2O$, **b:** $CdCl_2 \cdot H_2O$, **c**: $Cu(ClO_4)_2 \cdot 6H_2O$, **d**: $CuCl_2$ **e**: $CoCl_2 \cdot 2H_2O$. ***DMSO*** *has no effect.*

acid (2 mL) was added, resulting in the formation of a white precipitate (required product). Yield: 0.69 g (86%). M.p. > 260 °C. ^{1}H NMR (300 MHz, DMSO-d_6, δ (ppm)): 6.63 (s, 1H, NH Tetra); 6.18 (s, 1H, pz-H); 5.71 (s, 1H, pz-H); 2.56 (s, 3H, –CH_3); 2.51 (s, 2H, CH_2-Tetra); 2.14 (s, 3H, –CH_3); 1.89 (s, 3H, –CH_3). ^{13}C NMR (50 MHz, DMSO-d_6): 155.90 (1 C, C–NH, Tetra); 149.97 (1 C, C–CH_3); 145.84 (1 C, C–N); 145.27 (1 C, C–CH_3); 140.75 (1 C, C–CH_3); 109.38 (1 C, C=C, pz); 95.72 (1 C, C=C, pz); 43.87 (1 C, –CH_2-Tetra); 12.65 (1 C, –CH_3); 12.40 (1 C, –CH_3); 11.57 (1 C, –CH_3). Selected IR frequencies (KBr disc, cm^{-1}): 3137 (w), 2920 (w), 2070 (s), 1642 (m), 1553 (s). ESI-MS (+) *m/z*: 259.14136 $(M+H)^+$.

Synthesis of $[Ni(\mathbf{L1})_3](ClO_4)_2$ (**1**). 64.5 mg of **L1** (0.3 mmol, 3 eq.) was dissolved in acetonitrile (2.5 mL). To this solution, $Ni(ClO_4)_2 \cdot 6H_2O$ (36.56 mg, 0.1 mmol, 1 eq.) in acetonitrile (2.5 mL) was added. The reaction mixture was stirred for 10 min. Blue crystals suitable for X-ray diffraction analysis were obtained by vapor diffusion of diethyl ether into the reaction mixture after 4 days. Yield: 10.53 mg (10%). Selected IR frequencies (KBr disc, cm^{-1}): 3160 (w), 2993 (w), 2349

Research Article
doi.org/10.1002/ejic.202300634

Table 2. Anti-fusarium activity of complexes **2**, **5** and other model metal complexes.

Anti-fusarium activity – Co and Cd complexes	Concentration (μmol/L)	Inhibition (%)	Ref.
5	81.1	97	This work
2	97.75	51	
$[Co(SB)_2(bipy\text{-}amine)]$[g]	533.31	51	61
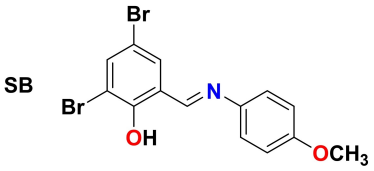			
$[Cd(SB)_2(bipy\text{-}amine)]$[g]	504.54	51	61
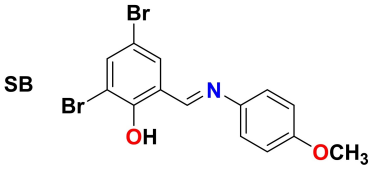			
$[Co(SB)_2(benen)]$[g]	498.73	61	61
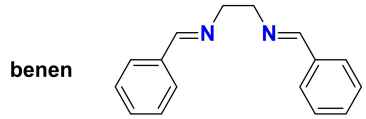			
$[Cd(SB)_2(benen)]$[g]	473.48	53	61
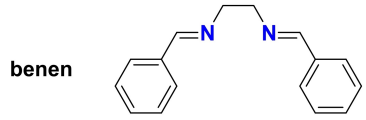			
$[Co(SB)_2(acphen)]$[g]	593.16	61	61
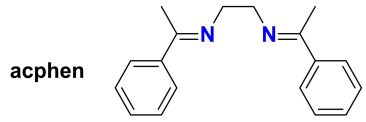			
$[Cd(SB)_2(acphen)]$[g]	557.79	61	61
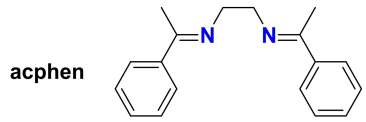			
$[CoL(CH_3OH)(H_2O)](ClO_4)_2$[h]	68.7	29	25
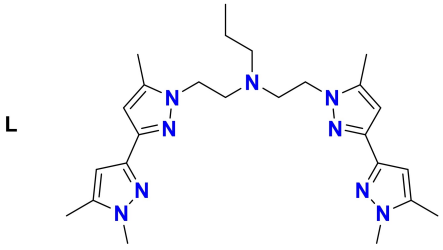			
$[Co(bssdh)]Cl$[i]	933.71	58	62
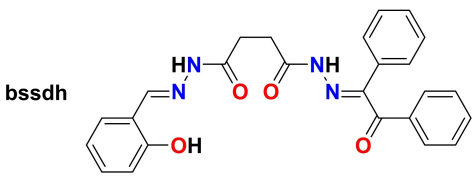			

Research Article
doi.org/10.1002/ejic.202300634

Table 2. continued

Anti-fusarium activity – Co and Cd complexes	Concentration (μmol/L)	Inhibition (%)	Ref.
[Cd(bssdh)]Cl[i]	848.9	68	62
bssdh 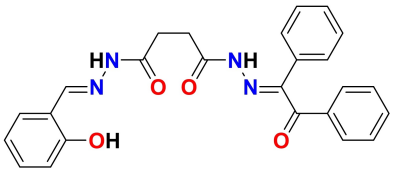			
[Co(dspdh)]Cl[j]	1088.14	55	62
dspdh 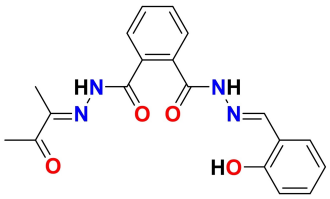			
[Cd(dspdh)]Cl[j]	974.66	67	62
dspdh 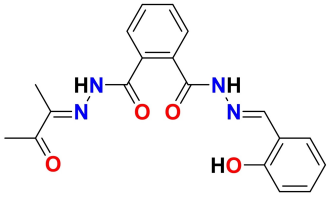			

[g] SB = 3,5-Dibromosalicylidene-p-anisidine. [h] L = *N*, *N* -bis(2(1′,5,5′-triméthyl–1 *H*, 1′ *H* -[3,3′-bipyrazol]-1-yl)ethyl)propan-1-amine. [I] bssdh = benzil salicylaldehyde succinic acid dihydrazone, [j] Hdspdh = diacetyl salicylaldehyde phthalic acid dihydrazone.

(w), 1556 (s). ESI-MS (+): *m/z* found = 351.6428, *m/z* calcd. for $[Ni(\mathbf{L1})_3]^{2+}$ = 351.64277; *m/z* found = 493.1633, *m/z* calcd. for $([Ni(\mathbf{L1})(ClO_4)_2] + Na)^+$ = 493.93868; *m/z* found = 587.1177, *m/z* calcd. for $([Ni(\mathbf{L1})_2(ClO_4)])^+$ = 587.11750. Anal. Calcd. for $\mathbf{1}\cdot H_2O$ ($C_{33}H_{41}N_{15}NiCl_2O_9$): C, 43.02; H, 4.49; N, 22.82; O, 15.63. Found: C, 42.88; H, 4.23; N, 22.61; O, 15.60.

Synthesis of $[Cd(\mathbf{L1})_2Cl_2]$ (**2**). A methanolic solution (with a few drops of water) containing $CdCl_2\cdot H_2O$ (21.1 mg, 0.1 mmol, 1 eq.) was added dropwise to a hot methanol solution (4 mL) of **L1** (64.5 mg, 0.3 mmol, 3 eq.). A white precipitate began to form after a few minutes. This precipitate was filtered and recrystallized in a water/acetonitrile mixture (1:1) to give clear crystals after slow solvent evaporation. Yield: 10.38 mg (17%). ^{1}H NMR (600 MHz, DMSO-d_6, δ (ppm)): 8.69 (s, 1H), 6.12 (s, 1H), 5.63 (s, 2H, CH_2–CN), 2.43 (s, 3H, –CH_3), 2.19 (s, 3H, –CH_3). ^{13}C NMR (151 MHz, DMSO-d_6, δ (ppm)): 157.59 (1 C, C–CH_3), 149.68 (1 C, C–N), 145.73 (1 C, C–CH_3),141.17 (1 C, C–CH_3), 115.01 (1 C, C≡N), 108.06 (1 C, C=C, pz), 37.54 (1 C, –CH_2–CN); 13.24 (1 C, –CH_3); 12.35 (1 C, –CH_3). Selected IR frequencies (KBr disc, cm^{-1}): 3131 (w), 2957 (w), 2333 (w), 1557 (s). ESI-MS (+): *m/z* found = 579.1056, *m/z* calcd for $[Cd(\mathbf{L1})_2Cl]^+$: 579.10561. Anal. Calcd. for **2** ($C_{22}H_{26}N_{10}CdCl_2$): C, 43.05; H, 4.27; N, 22.82. Found: C, 43.27; H, 4.23; N, 22.77.

Synthesis of $[Cu(\mathbf{HL2})(\mathbf{L2})]ClO_4$ (**3**)**. HL2** (51.6 mg, 0.2 mmol, 2 eq.) was dissolved in dilute perchloric acid (5%, 3 mL) at room temperature. $Cu(ClO_4)_2\cdot 6H_2O$ (37 mg, 0.1 mmol, 1 eq.) was dissolved in perchloric acid (5%, 2 mL) and immediately added to **HL2**, giving a clear green solution. This solution was stirred for 3 min at 60 °C and allowed to crystallize by slow solvent evaporation. Small green block crystals were collected after 2 days. Yield: 16.88 mg (25%). Selected IR frequencies (KBr disc, cm^{-1}): 3158 (w), 2926 (w), 2355 (m), 1730 (m), 1556 (s). ESI-MS (+): *m/z* found = 600.1718; *m/z* calcd. For $([Cu(\mathbf{L2})_2] + Na)^+$: 600.17145; ESI-MS (−): *m/z* found = 676.1346; *m/z* calcd. For $[Cu(\mathbf{L2})_2(ClO_4)]^-$: 676.1307. Anal. Calcd. For $\mathbf{3}\cdot 2HClO_4$ ($C_{22}H_{29}N_{16}CuCl_3O_{12}$): C, 30.05; H, 3.32; N, 25.48. Found: C, 31.44; H, 3.39; N, 25.91.

Synthesis of $[Cu(\mathbf{L2})_2]$ (**4**)**. HL2** (51.6 mg, 0.2 mmol, 2 eq.) was dissolved in diluted hydrochloric acid (5%, 3 mL) at room temperature. Cu^{II} chloride (13.4 mg, 0.1 mmol, 1 eq.) was dissolved in hydrochloric acid (5%, 2 mL) and immediately added to **HL2**, resulting in a dark green solution. This solution was stirred for 3 min at 60 °C and left to crystallize. Small dark green crystals were collected by filtration after 3 days and dried in air. Yield: 14.44 mg (25%). Selected IR frequencies (KBr disc, cm^{-1}): 3149 (w), 2922(w), 2351(m), 1559 (s ESI-MS (+): *m/z* found = 578.1893; *m/z* calcd. for $[Cu(\mathbf{HL2})(\mathbf{L2})]^+$: 578.18951. ESI-MS (+): *m/z* found = 600.1714; *m/z* calcd. for $([Cu(\mathbf{L2})_2] + Na)^+$: 600.17145. ESI-MS (+): *m/z* found = 616.1451; *m/z* calcd. for $([Cu(\mathbf{L2})_2] + K)^+$: 616.14539. ESI-MS (−): *m/z* found = 612.1530; *m/z* calcd. for $[Cu(\mathbf{L2})Cl]^-$: 612.15163. Anal. Calcd. for $\mathbf{4}\cdot 2H_2O\cdot 4HCl$ ($C_{22}H_{34}N_{16}CuCl_4O_2$): C, 34.77; H, 4.51; N, 29.49; Found: C, 34.91; H, 3.60; N, 29.57.

Synthesis of $[Co_2(\mathbf{HL2})(\mathbf{L2})Cl_3]$ (**5**). Solution of **HL2** (51.6 mg, 0.2 mmol, 2 eq.) in (5%, 3 mL) hydrochloric acid was added slowly to a dilute hydrochloric acid solution (5%, 2 mL) of $CoCl_2\cdot 6H_2O$ (23,7 mg, 0.1 mmol, 1 eq.). The resulting solution was stirred at 60 °C for 5 min. The reaction mixture was left for slow solvent evaporation, and pink coloured single crystals were obtained by filtration in air after 3 days. Yield: 22.1 mg (30%). Selected IR frequencies (KBr disc, cm^{-1}): 3137 (w), 2926(w), 2070 (m), 1636 (w), 1556 (s). ESI-MS (+): *m/z* found = 596.1757; *m/z* calcd. for $([Co(\mathbf{HL2})(\mathbf{L2})] + Na)^+$: 597.18287. ESI-MS (+): *m/z* found = 608.1571; *m/z*

calcd. for $[Co(\mathbf{L2})_2Cl]^-$: 608.15523. Anal. Calcd. For **5** ($C_{22}H_{27}Co_2Cl_3N_{16}$): C, 35.72; H, 3.68; N, 30.29. Found: C, 35.11; H, 3.63; N, 29.72.

Antimicrobial activities: Solid medium diffusion method (Mueller-Hinton medium, MHB) was used for antibacterial activity against strains (*Listeria innocua*, *E. Coli*, *Pseudomonas aeruginosa* and *Staphylococcus aureus*), and *Potato Dextrose medium* for antifungal activity against *Asperillus niger*, *Geotrichum candidum* and *Penicillium crustosum*.[73,74] The strains were diluted and adjusted to 0.5 McFarland, which corresponds to (10^6 CFU/ml for bacteria and 10^6 spores/mL for molds). Cultures were diluted with Mueller-Hinton broth for bacteria, and with sterile physiological water for molds. 0.1 mL of each diluted strain inoculated by surface spreading of the solid culture medium corresponding to each type of microorganism (bacteria or mold). 3 mg of each sample was dissolved in DMSO (1 mL) and was filled into the wells made on the solid medium. The dishes were then incubated for 2 h at 4 °C and then at 37 °C for 24 h for bacteria and at 25 °C for fungi. The diameters of the inhibition zones obtained around the wells were measured. Cycloheximide and Gentamicin were used as positive controls against fungi and bacteria, respectively.

Inhibition of *Fusarium* Growth: The final antifungal trial involved the following steps:

a. Preparation of PDA (Potato Dextrose Agar) culture medium: 39 g of PDA was added to distilled water (1 L). The mixture was refluxed for 10 min. Finally, the PDA medium was sterilized using an autoclave.
b. Preparation of the Foa (*Fusarium Oxysporum albidinis*) mushroom: Foa was isolated from xylem tissues exhibiting characteristic Bayoud disease symptoms. Vascular tissue fragments were cut off and aseptically put in PDA medium before being incubated at 28 °C. Fusarium oxysporum isolates were identified based on their morphological characteristics.[75,76] On PDA medium at 28 °C, one *Fusarium oxysporum* monoconidial was isolated.
c. Preparation of the samples and anti-Fusarium test: 4 mg of each molecule was solubilized in DMSO (1 mL). From this solution, 50 μL and 150 μL were placed in sterile tubes. Then, the sterile liquid PDA was added until reaching a total volume of 10 mL. The entire set was placed on Petri dishes with a 8.5 cm diameter, and the medium was allowed to stand until solidification.[77] In the middle of each Petri dish was a pellet of Foa that had already grown on the solid PDA. The dishes were incubated for four days at 28 °C. By comparing the diameter of the Foa to a control that contained only DMSO at some dose (control), the results are reported as a percentage of inhibition following eq. 1 as follows:[78]

$$\%\ of\ inhibition = \frac{D_0 - D_x}{D_0} * 100 \qquad \text{(eq. 1)}$$

D_0 = diameter (cm) of the Foa in the control.

D_x = diameter (cm) of the Foa in the test.

Author contributions

YB performed synthesis, characterization and wrote the paper with YG, MW and KR . SR and YG both designed and managed the project. MEIM and YD contributed to some organic syntheses. HNM, MF and KR undertook X-ray studies. RB and SO performed antibacterial and antifungal experiments. MW and KCH performed characterization of some samples.

Acknowledgements

This research was supported by the Fonds de la Recherche Scientifique-FNRS (PDR T.0095.21, CDR J.0064.23, J.0168.22,EQP U.N027.24), PPR2-MESRSFC-CNRSTP10 project (Morocco), and University of Glasgow, and the COST action CA21149. We thank CNRST Morocco and WBI Morocco for an excellence PhD stipendium as well as the ARES for a PhD scholarship allocated to YB.

Conflict of Interests

The authors declare no conflict of interest.

Data Availability Statement

The data that support the findings of this study are available from the corresponding author upon reasonable request.

Keywords: antimicrobial activity · bacteria · Bayoud disease · C,N-bipyrazole · *fusarium oxysporum* f. sp. *Albedinis* · tetrazole

[1] R. Ghomashi, S. Ghomashi, H. Aghaei, S. Massah, A. R. Massah, *Curr. Med. Chem.* **2023**, *30*, 4181–4255.
[2] I. D. Alshakova, G. I. Nikonov, *ChemCatChem* **2019**, *11*, 5370–5378.
[3] C. Verma, V. S. Saji, M. A. Quraishi, E. E. Ebenso, *J. Mol. Liq.* **2020**, *298*, 111943.
[4] S. Radi, A. Attayibat, M. El-Massaoudi, M. Bacquet, S. Jodeh, I. Warad, S. S. Al-Showiman, Y. N. Mabkhot, *Talanta* **2015**, *143*, 1–6.
[5] S. Radi, M. El Massaoudi, M. Bacquet, S. Degoutin, N. N. Adarsh, K. Robeyns, Y. Garcia, *Inorg. Chem. Front.* **2017**, *4*, 1821–1831.
[6] M. El-Massaoudi, S. Radi, M. Bacquet, S. Degoutin, Y. Garcia, *J. Environ. Chem. Eng.* **2018**, *6*, 5980–5989.
[7] S. Tighadouini, O. Roby, S. Mortada, Z. Lakbaibi, S. Radi, A. Al-Ali, M. E. A. Faouzi, M. Ferbinteanu, Y. Garcia, N. Al-Zaqri, A. Zarrouk, I. Warad, *J. Mol. Struct.* **2022**, *1247*, 131308.
[8] M. Cherfi, T. Harit, M. I. Yahyaoui, A. Asehraou, F. Malek, *Polycyclic Aromat. Compd.* **2022**, 1–12.
[9] Y. Draoui, S. Radi, M. El Massaoudi, Y. Bahjou, S. Ouahhoud, S. Mamri, M. Ferbinteanu, R. Benabbes, M. Wolff, K. Robeyns, Y. Garcia, *Molecules* **2023**, *28*, 6801.
[10] Y. Dong, Y. Liu, Q. Lyu, W. Huang, Y. Tang, *Cryst. Growth Des.* **2022**, *22*, 6140–6147.
[11] S. Manzoor, W. L. Cao, J. G. Zhang, *Def. Technol.* **2022**, *18*, 1945–1959.
[12] M. Friedrich, J. C. Gálvez-Ruiz, T. M. Klapötke, P. Mayer, B. Weber, J. J. Weigand, *Inorg. Chem.* **2005**, *44*, 8044–8052.
[13] S. Radi, M. El-Massaoudi, H. Benaissa, N. Adarsh, M. Ferbinteanu, E. Devlin, Y. Sanakis, Y. Garcia, *New J. Chem.* **2017**, *41*, 8232–8241.
[14] K. S. Kumar, S. Vela, B. Heinrich, N. Suryadevara, L. Karmazin, C. Bailly, M. Ruben, *Dalton Trans.* **2020**, *49*, 1022–1031.
[15] L. Sun, A. Rotaru, K. Robeyns, Y. Garcia, *Ind. Eng. Chem. Res.* **2021**, *60*, 8788–8798.
[16] L. Sun, A. Rotaru, Y. Garcia, *J. Hazard. Mater.* **2022**, *437*, 129364.
[17] Y. Huang, L. Z. Chen, R. G. Xiong, X. Z. You, *Inorg. Chim. Acta.* **2010**, *363*, 2512–2519.
[18] A. Frei, A. D. Verderosa, A. G. Elliott, J. Zuegg, M. A. T. Blaskovich, *Nat. Chem. Rev.* **2023**, *7*, 202–224.
[19] S. Monro, K. L. Colón, H. Yin, J. Roque, P. Konda, S. Gujar, R. P. Thumme, L. Lilge, C. G. Cameron, S. A. McFarland, *Chem. Rev.* **2019**, *119*, 797–828.

[20] L. Gourdon, K. Cariou, G. Gasser, *Chem. Soc. Rev.* **2022**, *51*, 1167–1195.
[21] T. A. Sales, I. G. Prandi, A. A. de Castro, D. H. S. Leal, E. F. F. da Cunha, K. Kuca, T. C. Ramalho, *Int. J. Mol. Sci.* **2019**, *20*, 1829–1862.
[22] C. N. Morrison, K. E. Prosser, R. W. Stokes, A. Cordes, N. Metzler-Nolte, S. M. Cohen, *Chem. Sci.* **2020**, *11*, 1216–1225.
[23] K. Chkirate, K. Karrouchi, N. Dege, N. K. Sebbar, A. Ejjoummany, S. Radi, N. N. Adarsh, A. Talbaoui, M. Ferbinteanu, E. M. Essassi, Y. Garcia, *New J. Chem.* **2020**, *44*, 2210–2221.
[24] K. Chkirate, K. Karrouchi, H. Chakchak, J. T. Mague, S. Radi, N. N. Adarsh, W. Li, A. Talbaoui, E. M. Essassi, Y. Garcia, *RSC Adv.* **2022**, *12*, 5324–5339.
[25] Y. Draoui, S. Radi, A. Tanan, A. Oulmidi, H. N. Miras, R. Benabbes, S. Ouahhoudo, S. Mamri, A. Rotaru, Y Garcia, *RSC Adv.* **2022**, *12*, 17755–17764.
[26] F. Shabani, L. Kumar, A. Esmaeili, *Agric. Ecosyst. Environ.* **2014**, *197*, 96–105.
[27] E. D. T. Bouhlali, M. Derouich, H. Ben-Amar, R. Meziani, A. Essarioui, *Scientifica* **2021**, 1896015.
[28] A. Dihazi, F. Jaiti, S. Jaoua, A. Driouich, M. Baaziz, F. Daayf, M. A. Serghini, *Plant Physiol. Biochem.* **2012**, *55*, 7–15.
[29] Y. Kaddouri, R. Benabbes, S. Ouahhoud, M. Abdellattif, B. Hammouti, R. Touzani, *Molecules* **2022**, *27*, 2698.
[30] Y. Kaddouri, F. Abrigach, S. Ouahhoud, R. Benabbes, M. El Kodadi, A. Alsalme, N. Al-Zaqri, I. Warad, R. Touzani, *Bioorg. Chem.* **2021**, *110*, 104696.
[31] P. P. Dholakiya, M. N. Patel, *Synth. React. Inorg. Met.-Org. Nano-Met. Chem.* **2002**, *32*, 819–829.
[32] A. Frei, J. Zuegg, A. G. Elliott, M. Baker, S. Braese, C. Brown, F. Chen, C. G. Dowson, G. Dujardin, N. Jung, A. P. King, A. M. Mansour, M. Massi, J. Moat, H. A. Mohamed, A. K. Renfrew, P. J. Rutledge, P. J. Sadler, M. H. Todd, C. E. Willans, J. J. Wilson, M. A. Cooper, M. A. T. Blaskovich, *Chem. Sci.* **2020**, *11*, 2627–2639.
[33] H. Ayada, B. Dhioui, H. Mazouz, A. El Harrak, F. Jaiti, B. Ouhmidou, M. Diouri, M. Moumni, *Sci. Rep.* **2022**, *12*, 19098.
[34] M. Marinozzi, G. Marcelli, A. Carotti, B. Natalini, *RSC Adv.* **2014**, *4*, 7019–7023.
[35] R. Ketkaew, Y. Tantirungrotechai, P. Harding, G. Chastanet, P. Guionneau, M. Marchivie, D. J. Harding, *Dalton Trans.* **2021**, *50*, 1086–1096.
[36] M. Buron-Le Cointe, J. Hébert, C. Baldé, N. Moisan, L. Toupet, P. Guionneau, J. F. Létard, E. Freysz, H. Cailleau, E. Collet, *Phys. Rev. B* **2012**, *85*, 39–41.
[37] M. G. B. Drew, C. J. Harding, V. McKee, G. G. Morgan, J. Nelson, *Chem. Commun.* **1995**, 1035–1038.
[38] M. Marchivie, P. Guionneau, J. F. Létard, D. Chasseau, *Acta Crystallogr.* **2005**, *B61*, 25–28.
[39] H. S. Ren, M. J. Ming, J. Y. Ma, X. Y. Li, *J. Phys. Chem. A* **2013**, *117*, 8017–8025.
[40] E. Collet, P. Guionneau, *C. R. Chim.* **2018**, *21*, 1133–1151.
[41] A. W. Addison, T. N. Rao, J. Reedijk, J. van Rijn, G. C. Verschoor, *J. Chem. Soc. Dalton Trans.* **1984**, 1349–1356.
[42] L. Yang, D. R. Powell, R. P. Houser, *Dalton Trans.* **2007**, 955–964.
[43] M. Wolff, D. J. Grimwood, J. J. McKinnon, M. J. Turner, D. Jayatilaka, M. A. Spackman, Crystal Explorer 17.5, University of Western Australia Crawley, Australia, **2012**.
[44] P. R. Spackman, M. J. Turner, J. J. McKinnon, S. K. Wolff, D. J. Grimwood, D. Jayatilaka, M. A. Spackman, *J. Appl. Crystallogr.* **2021**, *54*, 1006–1011.
[45] M. N. Kumbar, R. R. Kamble, J. P. Dasappa, P. K. Bayannavar, H. A. Khamees, M. Mahendra, S. D. Joshi, S. Dodamani, V. Rasal, S. Jalalpure, *J. Mol. Struct.* **2018**, *1160*, 63–72.
[46] M. Azam, S. M. Wabaidur, M. Alam, A. Trzesowska-Kruszynska, R. Kruszynski, S. I. Al-Resayes, F. F. Alqahtani, M. R. Khan, *Polyhedron* **2021**, *195*, 114991.
[47] S. M. Soliman, A. El-Faham, S. E. El Silk, *Appl. Organomet. Chem.* **2020**, *34*, e5941.
[48] R. M. Irfan, M. A. Shaheen, M. Saleem, M. N. Tahir, K. S. Munawar, S. Ahmad, S. L. Rubab, T. Tahir, K. Kotwica-Mojzych, M. Mojzych, *Arab. J. Chem.* **2021**, *14*, 103308.
[49] N. Dharmaraj, P. Viswanathamurthi, K. Natarajan, *Transition Met. Chem.* **2001**, *26*, 105–109.
[50] A. Chaudhary, A. Phor, R. V. Singh, *Main Group Met. Chem.* **2003**, *178*, 603–613.
[51] L. H. Abdel-Rahman, A. M. Abu-Dief, R. M. El-Khatib, S. M. Abdel-Fatah, A. A. Seleem, *IJNC* **2016**, *2*, 83–91.
[52] M. Montazerozohori, S. A. Musavi, A. Masoudiasl, A. Naghiha, M. Dusek, M. Kucerakova, *Spectrochim. Acta A Mol. Biomol. Spectrosc.* **2015**, *137*, 389–396.
[53] N. M. Aghatabay, A. Neshat, T. Karabiyik, M. Somer, D. Haciu, B. Dülger, *Eur. J. Med. Chem.* **2007**, *42*, 205–213.
[54] E. Zangrando, M. S. Begum, M. C. Sheikh, R. Miyatake, M. M. Hossain, M. M. Alam, M. A. Hasnat, M. A. Halim, S. Ahmed, M. N. Rahman, A. Ghosh, *Arab. J. Chem.* **2017**, *10*, 172–184.
[55] M. Bouhdada, M. E. Amane, H. E. Hamdani, *J. Mol. Struct.* **2023**, *1271*, 134026.
[56] M. Pervaiz, I. Ahmad, M. Yousaf, S. Kirn, A. Munawar, Z. Saeed, A. Adnan, T. Gulzar, T. Kamal, A. Ahmad, A. Rashid, *Spectrochim. Acta Part A* **2019**, *206*, 642–649.
[57] D. Ashok, N. Nagaraju, B. V. Lakshmi, M. Sarasija, *Russ. J. Gen. Chem.* **2019**, *89*, 1905–1910.
[58] P. Ashokgajapathiraju, L. Ravindranath, J. Sreeramulu, *Res. J. Pharm. Biol. Chem. Sci.* **2014**, *5*, 179–186.
[59] Y. Allab, S. Chikhi, S. Zaater, M. Brahimi, S. Djebbar, *Inorg. Chim. Acta.* **2020**, *504*, 119436.
[60] H. Palza, *Int. J. Mol. Sci.* **2015**, *16*, 2099–2116.
[61] P. P. Dholakiya, M. N. Patel, *Synth. React. Inorg. Met.-Org. Nano-Met. Chem.* **2004**, *32*, 819–829.
[62] V. P. Singh, P. Gupta, *J. Enzyme Inhib. Med. Chem.* **2008**, *23*, 797–805.
[63] CrysAlisPro, version 1.171.33.49b, *Oxford Diffraction Ltd.* Abingdon, UK, 2009.
[64] G. M. Sheldrick, *Acta Crystallogr.* **2015**, *A71*, 3–8.
[65] G. M. Sheldrick, *Acta Crystallogr.* **2015**, *C71*, 3–8.
[66] A. L. Spek, *Acta Crystallogr.* **2015**, *C71*, 9–18.
[67] G. M. Sheldrick, *Acta Crystallogr.* **1990**, *46*, 467–473.
[68] G. M. Sheldrick, *Acta Crystallogr.* **2008**, *64*, 112–122.
[69] L. J. Farrugia, *J. Appl. Crystallogr.* **1999**, *32*, 837–838.
[70] R. C. Clark, J. S. Reid, *Acta Crystallogr.* **1995**, *51*, 887–897.
[71] A. Altomare, G. Cascarano, C. Giacovazzo, A. Guagliardi, *J. Appl. Crystallogr.* **1993**, *26*, 343–350.
[72] Crystal Structure 4.2: Crystal Structure Analysis Package, Rigaku Corporation (2000–2015). Tokyo 196–8666, Japan.
[73] J. K. Hurst, *Coord. Chem. Rev.* **2005**, *249*, 313–328.
[74] D. Chatterjee, A. Mitra, R. E. Shepherd, *Inorg. Chim. Acta.* **2004**, *357*, 980–990.
[75] P. E. Nelson, *Mycopathologia* **1992**, *117*, 29–36.
[76] C. Booth, Y. Clayton, M. Usherwood, *Proceed.: Plant Sciences* **1985**, *94*, 433–436.
[77] F. Neri, M. Mari, S. Brigati, *Plant Pathol.* **2006**, *55*, 100–105.
[78] A. Hmouni, M. Hajlaoui, A. Mlaiki, *Bull. OEPP.* **1996**, *26*, 697–705.

Manuscript received: November 10, 2023
Revised manuscript received: November 21, 2023
Version of record online: December 21, 2023